Singularity and universality from von Neumann to Rényi entanglement entropy and disorder operator in Motzkin chains

Jianyu Wang,[1,2,3,4,5] Zenan Liu,[6,5] Zheng Yan,[6,5,*] and Congjun Wu[2,3,4,5,†]

[1]*State Key Laboratory of Surface Physics and Department of Physics, Fudan University, Shanghai 200438, China*

[2]*New Cornerstone Science Laboratory, Department of Physics, School of Science, Westlake University, Hangzhou 310024, China*

[3]*Institute for Theoretical Sciences, Westlake University, Hangzhou 310024, China*

[4]*Key Laboratory for Quantum Materials of Zhejiang Province, School of Science, Westlake University, Hangzhou 310024, China*

[5]*Institute of Natural Sciences, Westlake Institute for Advanced Study, Hangzhou 310024, China*

[6]*Department of Physics, School of Science and Research Center for Industries of the Future, Westlake University, Hangzhou 310030, China*

(Received 4 March 2025; revised 22 July 2025; accepted 25 July 2025; published 14 August 2025)

Rényi entanglement entropy is widely used to study quantum entanglement properties in strongly correlated systems, and its analytic continuation as the Rényi index $n \to 1$ is often believed to yield von Neumann entanglement entropy. However, earlier theoretical analysis indicated that this process exhibits a singularity for the colored Motzkin spin chain problem, leading to different system size l scaling behaviors of $\sim\sqrt{l}$ and $\sim \ln l$ for the von Neumann and Rényi entropies, respectively. Our analytical and numerical calculations confirm this transition, which can be explained by the exponentially increasing density of states in the entanglement spectrum we extract numerically. Moreover, disorder operators can be measured easily in numerics and experiments and always have area-law or volume-law scaling similar to entanglement entropies. We further explored disorder operators under various symmetries of such a system. Both analytical and numerical results demonstrate that the scaling behaviors of disorder operators also follow $\ln l$ as the leading term, matching that of Rényi entropy. Moreover, we find that the coefficient of the term $\ln l$ is a universal constant shared by both the Rényi entropy and disorder operators and propose that it can probe the underlying constraint physics of Motzkin walks.

DOI: 10.1103/wffk-7ycs

I. INTRODUCTION

In recent years, the interflow and mutual learning between condensed matter and quantum information have inspired increasingly fruitful research [1–3]. In the field of quantum information, the entanglement entropy (EE) plays a key role in measuring information and chaos [4,5]. As one of the basic properties of quantum mechanics, quantum entanglement itself is difficult to measure. Moreover, the introduction of EE in condensed matter physics has revealed rich physics, such as topological entanglement entropy and long-range entanglement in highly entangled matter [6,7]. One important topic in condensed matter physics is using EE to probe the intrinsic physics of many-body systems [6–10]. Among many intriguing features, EE offers a direct connection between the conformal field theory (CFT) and categorical description of the problems beyond traditional observables [11–25].

Unlike in few-body systems, the scaling behaviors of EE in quantum many-body systems reveal universal properties, such as the central charge [11,26–28], number of Goldstone modes [29–32], and quantum dimension of topological order [6,7,33,34]. Within the framework of CFT [15,35–38], the EE with corner cuts in two-dimensional quantum systems usually obeys the area law $s = al + b\ln l + \delta$, where l is the length of the entangled boundary, b is related to the angles of the corners, and a is generally thought to be UV dependent. Meanwhile, the coefficients b and δ are usually employed to extract universal information and detect novel phases and criticalities [2].

The von Neumann (vN) EE $s_A^{\mathrm{vN}} = -\mathrm{Tr}(\rho_A \ln \rho_A)$ (ρ_A is the reduced density matrix) as the generalization of Shannon entropy in quantum mechanics is widely used to study the above questions [39–42]. However, due to the difficulty in the calculation of vN EE, Rényi EE is much more commonly used in both field theory and numerical calculations. The definition of Rényi EE is $s_A^{(n)} = \frac{1}{1-n}\ln[\mathrm{Tr}(\rho_A^n)]$, where n is the Rényi index. Formally, Rényi EE will become vN EE as $n \to 1$. Although the Rényi EE loses certain properties, such as additivity and subadditivity [43–47], it is strongly believed to yield the same scaling behaviors as the vN EE, e.g., the area and volume laws. It was generally believed in the past that all the coefficients of vN EE for each $O(l)$ scaling term can be obtained via the analytic continuation of $n \to 1$ [26,48,49]. For numerous examples, including both theoretical and numerical results, this common belief has been massively tested [50,51].

However, the colored Motzkin spin chain was found to be a counterexample [52–54]. There is a singularity in the limit of Rényi index $n \to 1$, in which the coefficient of the leading term $\ln l$ will be divergent. It actually indicates that an extra term, $\sqrt{l}$, becomes the leading term in the vN EE. This result provides a counterexample of the analytic continuation from Rényi to von Neumann EE, which cautions that people should be careful when studying EE.

*Contact author: zhengyan@westlake.edu.cn

†Contact author: wucongjun@westlake.edu.cn

On the other hand, the disorder operator (DO) is a nonlocal observable similar to the EE which has been proposed to extract the high-form symmetry and CFT information of quantum many-body systems [23,55–57]. It has been successfully used to detect high-form symmetry breaking at the Ising transition [22]. The current central charges in CFT can be captured by the DO at phase transitions of the $O(2)$ and $O(3)$ universal classes in (2+1) dimensions [58,59]. DOs have also been designed in fermionic systems to explore the universal features of Fermi liquids, Luttinger liquids, and quantum critical points in fermionic systems [60–62]. The DO satisfies universal scaling behaviors similar to those in EE, where the logarithmic term usually reflects general features of CFT. Moreover, based on its definition, the expectation value of twisting the symmetry within the subsystem region is straightforward to measure numerically and is more easily measured in experiments than EE [60].

In this article, we systematically study the scaling behaviors of the vN and Rényi EEs of a one-dimensional (1D) colored Motzkin spin chain with different spins S both analytically and numerically. The scaling behaviors of DOs for the Motzkin spin chain are also investigated and are found to be similar to those of the Rényi EE. The numerical data are available from Ref. [63]. Moreover, we find that the coefficient of the logarithmic term is universal for any spin value, regardless of the DO or Rényi EE.

This paper is organized as follows: In Sec. II, the background of the Motzkin chain is presented. In Sec. III, the analytic solution of EE is given, encompassing an analysis of Rényi EE to facilitate further discussion. In Sec. IV, we introduce the algorithm for Monte Carlo simulations and provide a detailed discussion of the numerical results for entanglement entropies. In Sec. V, we focus on the disorder operators of the Motzkin chain, exploring both analytical and numerical perspectives, and reveal that these disorder operators lead by $\frac{3}{2}\ln l$. The summary and conclusion are presented in Sec. VI.

II. BACKGROUND OF MOTZKIN CHAINS

In this section, we review the concept of the Motzkin chain, which is a 1D spin chain inspired by the Motzkin path from combinatorial mathematics [64,65].

The Motzkin walk or Motzkin path is a kind of nonnegative lattice path defined as follows. Random walks starting from the point (0,0) and ending at $(2l, 0)$ on a two-dimensional x-y plane, as shown in Fig. 1, consist of three types of steps: upward steps ／, downward steps ＼, and horizontal steps —, represented as vectors (1,1), $(1,-1)$, and (1,0), respectively. Then Motzkin walks are those random walks that do not cross below the x axis ($y = 0$). Bravyi *et al.* [66] introduced a frustrated-free spin-1 chain model whose unique ground state is the equal-weight superposition of all Motzkin walk states, achieved by mapping the spin S^z states $\{\uparrow, 0, \downarrow\}$ to the steps {／, —, ＼}, respectively. Movassagh and Shor [52] then generalized this model into an S-color Motzkin model, where the upward or downward steps are colored using S different colors. This model can be translated to a spin-S quantum chain. An example of the two-color Motzkin walk is shown in Fig. 1. For a 1D S-color Motzkin model of size $2l$, the Hamiltonian is constructed by local projection

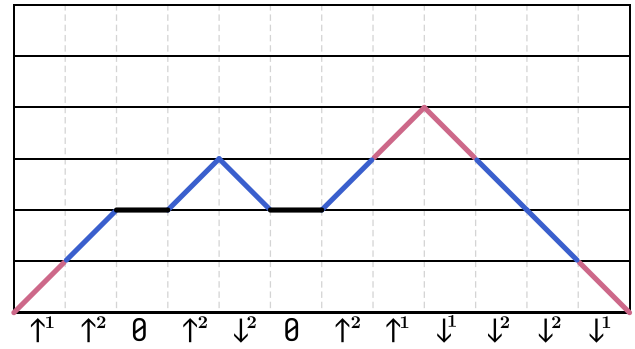

FIG. 1. Example of a two-color Motzkin walk (colored path). The walk starts and ends on the x axis and cannot cross below it. It can be mapped to an S^z configuration of a spin-2 chain (shown below the x axis). The pink upward and downward steps are mapped to $S^z = \pm 1$, the blue steps are mapped to $S^z = \pm 2$, and the black horizontal steps are mapped to $S^z = 0$.

operators in the following form:

$$H = \Pi^{\text{boundary}} + \sum_{j=1}^{2l-1} \Pi^{\text{cross}}_{j,j+1} + \sum_{j=1}^{2l-1} \Pi^{\text{exchange}}_{j,j+1}, \tag{1}$$

with

$$\begin{aligned}
\Pi^{\text{boundary}} &= \sum_{k=1}^{S} (|\downarrow^k\rangle_{1,1} \langle\downarrow^k| + |\uparrow^k\rangle_{2l,2l} \langle\uparrow^k|), \\
\Pi^{\text{cross}}_{j,j+1} &= \sum_{k\neq k'}^{S} |\uparrow^k\downarrow^{k'}\rangle_{j,j+1} \langle\uparrow^k\downarrow^{k'}|, \\
\Pi^{\text{exchange}}_{j,j+1} &= \sum_{k=1}^{S} |D^k\rangle_{j,j+1} \langle D^k| + |U^k\rangle_{j,j+1} \langle U^k| \\
&\quad + |V^k\rangle_{j,j+1} \langle V^k|,
\end{aligned} \tag{2}$$

where the superscript k indicates colors, i.e., $\uparrow^k$ stands for the $S^z = k$ state and $\downarrow^k$ stands for the $S^z = -k$ state. The boundary term Π^{boundary} ensures that the first and last steps do not pass below the x axis. The cross term Π^{cross} keeps the correct order of different color pairs. As a counterexample, $\uparrow^k\uparrow^{k'}\downarrow^k\downarrow^{k'}$ is not allowed if $k \neq k'$. The exchange term Π^{exchange} contains states $|D^k\rangle = \frac{\sqrt{2}}{2}(|\downarrow^k 0\rangle - |0\downarrow^k\rangle)$, $|U^k\rangle = \frac{\sqrt{2}}{2}(|\uparrow^k 0\rangle - |0\uparrow^k\rangle)$, and $|V^k\rangle = \frac{\sqrt{2}}{2}(|\uparrow^k\downarrow^k\rangle - |00\rangle)$, which leads to the step exchange of

／— ↔ —／, ＼— ↔ —＼, ／＼ ↔ ——. (3)

Notice that there is no such step exchange as

＼／ ↔ ——. (4)

This property ensures that the walk height remains nonnegative.

The ground state of the Hamiltonian (1) is the superposition of all the Motzkin walk configurations $|M_i\rangle$ [66],

$$|G\rangle = \frac{1}{\sqrt{N}} \sum_{i}^{N} |M_i\rangle, \tag{5}$$

where N is the number of all the Motzkin walks allowed.

III. THE EE OF COLORED MOTZKIN CHAINS

The EE between two subsystems obtained by cutting the Motzkin chain at the midpoint is analytically studied in this section. It is worth noting that similar results were studied in Refs. [52,53]; i.e., the vN EE and Rényi EE of colored Motzkin chains exhibit different scalings. In order for this article to be easily readable and self-contained, we present the calculation of the Rényi EE here. In addition, our analytical method is different from those in the literature.

Consider an S-color Motzkin chain with a size of $2l$. The vN EE of half cutting takes the form [52]

$$s^{\mathrm{vN}} = a\sqrt{l} + b\ln l + \mathrm{const}, \tag{6}$$

with

$$a = 2\sqrt{\frac{2\sqrt{S}}{(2\sqrt{S}+1)\pi}}\ln S, \quad b = \frac{1}{2}. \tag{7}$$

The Rényi EE ($n > 1$) is [53]

$$s^{(n)} = b\ln l + \mathrm{const}, \tag{8}$$

with

$$b = \frac{3}{2}\left(1 + \frac{1}{n-1}\right). \tag{9}$$

The vN and Rényi EEs exhibit different scaling behaviors. For comparison, when $S = 1$ (the colorless case), the leading terms of both the vN EE and Rényi EE are $\frac{1}{2}\ln l$. As a notation, "ln" in this article stands for the natural logarithm.

For the completeness of the article and convenience in further analyses, we provide the derivation of the Rényi EE $s^{(n)}$. The analysis below elucidates the emergence of a singularity at $n \to 1$, where the vN and Rényi EEs exhibit distinct scaling regimes governed by discontinuous analytic continuations.

A. Analytical calculation of Rényi EE

Given the ground state wave function of Eq. (5), the reduced density matrix's eigenvalues under half cutting are [52]

$$\lambda_m \simeq \frac{S^{-m}}{T}\frac{m^2}{l}e^{-\frac{1}{2}(2+\frac{1}{\sqrt{S}})\frac{m^2}{l}}, \tag{10}$$

where the index m takes integer values from 0 to l, corresponding to the midpoint height of a Motzkin walk. The degeneracy of the eigenvalue λ_m is S^m; thus, we define $\Lambda_m = S^m\lambda_m$. And λ_m reaches its maximum at an intermediate value of m. Additionally, T is a normalization factor that ensures $\sum_m S^m\lambda_m = 1$.

The nth Rényi EE is then given by

$$\begin{aligned} s^{(n)} &= \frac{1}{1-n}\ln\sum_{m=0}^{l} S^m\lambda_m^n \\ &= \frac{1}{1-n}\ln\sum_{m=0}^{l}\frac{S^{(1-n)m}}{T^n}\frac{m^{2n}}{l^n}e^{-\frac{n}{2}(2+\frac{1}{\sqrt{S}})\frac{m^2}{l}}. \end{aligned} \tag{11}$$

Setting $\xi = m/\sqrt{l}$ and using the integral approximation to Eq. (11), the Rényi EE ($n > 1$) is expressed as

$$\begin{aligned} s^{(n)} \simeq \frac{1}{2}\ln l + \frac{1}{1-n}\ln\Bigg\{\tilde{T}^{-n}\int_0^{\sqrt{l}} d\xi\,\xi^{2n} \\ \times\exp\left[-\frac{n}{2}\left(2+\frac{1}{\sqrt{S}}\right)\xi^2 - (n-1)\ln(S)\sqrt{l}\,\xi\right]\Bigg\}, \end{aligned} \tag{12}$$

where

$$\tilde{T} = \frac{T}{\sqrt{l}} \simeq \int_0^{\sqrt{l}} d\xi\xi^2\exp\left[-\frac{1}{2}\left(2+\frac{1}{\sqrt{S}}\right)\xi^2\right]. \tag{13}$$

For the case with $n > 1$, the Rényi EE can be simplified to

$$s^{(n)} = \frac{1}{2}\ln l - \frac{n}{1-n}\ln\tilde{T} + R, \tag{14}$$

where

$$\begin{aligned} R = \frac{1}{1-n}\ln\int_0^{\sqrt{l}} d\xi\,\xi^{2n}\exp\Bigg[-\frac{n}{2}\left(2+\frac{1}{\sqrt{S}}\right)\xi^2 \\ -(n-1)\ln(S)\sqrt{l}\,\xi\Bigg]. \end{aligned} \tag{15}$$

For convenience, the following functions are defined: Functions p_1 and p_2 are defined as

$$\begin{aligned} p_1(n,S) &= \frac{n}{2}\left(2+\frac{1}{\sqrt{S}}\right), \\ p_2(n,S) &= (n-1)\ln(S). \end{aligned} \tag{16}$$

The function F_α is defined as

$$F_\alpha(p_1,p_2,l) = \int_0^{\sqrt{l}} d\xi\xi^\alpha\exp\left[-p_1\xi^2 - p_2\sqrt{l}\,\xi\right]. \tag{17}$$

Consequently, in the large-l limit, R in Eq. (15) is expressed as

$$R = \frac{1}{1-n}\ln F_{2n}. \tag{18}$$

The positive function F_α has the limit of $\lim_{l\to\infty}F_\alpha \to 0$. Additionally, we can easily establish the following relations for the large-l limit:

$$\frac{d}{dl}F_\alpha = -\frac{p_2}{2\sqrt{l}}F_{\alpha+1}, \tag{19}$$

$$(\alpha+1)F_\alpha = p_2\sqrt{l}F_{\alpha+1} + 2p_1F_{\alpha+2}. \tag{20}$$

Because F_α and f are positive and p_2 is also positive for the condition $n, S > 1$, the following limit can be proved according to Eq. (20):

$$\lim_{l\to\infty}\frac{F_\alpha}{F_{\alpha+1}} > \lim_{l\to\infty}\frac{p_2\sqrt{l}}{\alpha+1} = +\infty. \tag{21}$$

Thus, for large enough l we have the relation

$$F_\alpha \simeq \frac{p_2\sqrt{l}}{\alpha+1}F_{\alpha+1}. \tag{22}$$

B. The scaling form of Rényi EE

Now we analyze the scaling of Rényi EE in Eq. (14). The first term contributes a logarithmic scaling obviously. The second term contributes a constant because $\tilde{T}$ has an upper bound in the limit $l \to \infty$, which is

$$\lim_{l\to\infty} \tilde{T} = \sqrt{\frac{\pi}{2}}\left(2+\frac{1}{\sqrt{S}}\right)^{-\frac{3}{2}}. \tag{23}$$

Then only the third term, R, needs to be calculated.

Using L'Hôpital's rule and Eqs. (19), (20), and (21), we have

$$\begin{aligned}\lim_{l\to\infty}\frac{R}{\ln(l)} &= \frac{2n+1}{2n-2}\lim_{l\to\infty}\frac{p_2\sqrt{l}F_{2n+1}}{p_2\sqrt{l}F_{2n+1}+p_1F_{2n+2}}\\ &= \frac{2n+1}{2n-2}.\end{aligned} \tag{24}$$

This indicates that the scaling of R is given by

$$R = \frac{2n+1}{2n-2}\ln l + C, \tag{25}$$

where

$$\begin{aligned}C &= \lim_{l\to\infty}\left(R-\frac{2n+1}{2n-2}\ln l\right)\\ &= \frac{1}{1-n}\lim_{l\to\infty}\ln\left(l^{\frac{2n+1}{2}}F_{2n}\right).\end{aligned} \tag{26}$$

According to Eq. (22), the limit of the term in the logarithm function is

$$\lim_{l\to\infty} l^{\frac{2n+1}{2}}F_{2n} = \frac{\Gamma(2n+1)}{p_2^{2n}}\lim_{l\to\infty}\sqrt{l}F_0 = \frac{\Gamma(2n+1)}{p_2^{2n+1}}, \tag{27}$$

where Γ is the gamma function. Then C is a constant in the large-l limit:

$$C = \frac{1}{1-n}\ln\left(\frac{\Gamma(2n+1)}{p_2^{2n+1}}\right). \tag{28}$$

In short, by substituting Eqs. (23), (25), and (28) into Eq. (14), the expression of Rényi EE (for $n > 1$ and $S > 1$) in the large-l limit becomes [53]

$$s^{(n)} = \frac{3}{2}\left(1+\frac{1}{n-1}\right)\ln l + \delta, \tag{29}$$

where the constant δ is

$$\begin{aligned}\delta = \frac{1}{(n-1)}\Bigg\{&\frac{n}{2}\ln\frac{\pi}{2} - \frac{3n}{2}\ln\left(2+\frac{1}{\sqrt{S}}\right)\\ &-\ln\Gamma(2n+1)+(2n+1)\ln\left[(n-1)\ln S\right]\Bigg\}.\end{aligned} \tag{30}$$

By comparing Eq. (29) with the scaling form of EE in CFT, we propose that the coefficient of $3/2$ in the logarithmic term of the Rényi EE is universal for arbitrary S, while the constant term δ is complex and nonuniversal.

IV. NUMERICAL RESULT OF EE

Monte Carlo (MC) simulations have been widely used to calculate Rényi EE in quantum many-body systems in recent years [24,25,32,67–75]. In this section, we use the MC method to estimate the scaling behaviors of the vN and Rényi EEs in the Motzkin chain.

Our simulation is based on the SWAP operator method. For pure states that can be written as the product states of two subsystems A and B, the SWAP_A operator is defined as

$$\begin{aligned}&\text{SWAP}_A(|A_1\rangle\otimes|B_1\rangle)(|A_2\rangle\otimes|B_2\rangle)\\ &\quad= (|A_2\rangle\otimes|B_1\rangle)(|A_1\rangle\otimes|B_2\rangle).\end{aligned} \tag{31}$$

The ground state expectation value of the SWAP_A operator is the second-order Rényi EE [67,72,76],

$$s_A^{(2)} = -\ln\text{Tr}\left(\rho_A^2\right) = -\ln\langle\text{SWAP}_A\rangle, \tag{32}$$

where $\langle\cdots\rangle$ indicates the expectation value with respect to the replica ground state,

$$|G\rangle^2 \equiv |G\rangle\otimes|G\rangle\,. \tag{33}$$

Based on properties of the ground states of the colored Motzkin chain, our algorithm can be simplified, and then its accuracy significantly improved. The details of the algorithm are provided below.

A. The Monte Carlo algorithm

The MC algorithm used to estimate the EE is presented below. The ground state given in Eq. (5) is positive definite; hence, the expectation value of the SWAP_A operator in Eq. (32) can be written as

$$\langle\text{SWAP}_A\rangle = \sum_{i_1,i_2}\frac{1}{N}\langle G|^2\,\text{SWAP}_A\,|M_{i_1}\rangle\otimes|M_{i_2}\rangle\,. \tag{34}$$

Based on this formula, it is straightforward to set up a MC algorithm to calculate the second-order Rényi EE $s^{(2)}$. One can simulate two replicas of configurations M_{i_1} and M_{i_2} with equal weights and measure the value of the estimator

$$\langle G|^2\,\text{SWAP}\,|M_{i_1}\rangle\otimes|M_{i_2}\rangle\,. \tag{35}$$

However, the symmetries of the colored Motzkin chain ground state allow us to further simplify the algorithm, so that only one replica needs to be sampled. In this work, we consider a Motzkin chain of size $2l$ and study the EE of the subsystem by cutting at the midpoint. The length of subsystem A is constrained to l throughout the discussion below.

The swappability of Motzkin walks can be defined as follows. Exchanging half of the path of walks M_1 and M_2 generates two new walks denoted as $\tilde{M}_1$ and $\tilde{M}_2$. We assert that M_1 is swappable with M_2 if $\tilde{M}_1$ also qualifies as a Motzkin walk. It is easy to identify the following properties of the Motzkin walk swappability: (1) If M_1 is swappable with M_2, then M_2 is also swappable with M_1. (2) If M_1 is swappable with M_2 and M_2 is swappable with M_3, it follows that M_1 is swappable with M_3. Consequently, we can conclude that the measurement variable in Eq. (35) has only two possible values: It takes a value of 1 if M_{i_1} and M_{i_2} are swappable; otherwise, it takes a value of zero.

Colored Motzkin walks can then be categorized into classes c_m based on their swappability—walks within each class c_m are swappable with each other. In this context, m represents the height at the midpoint, which corresponds to the number of unpaired steps in half of the Motzkin walks. Notably, there are S^m equivalent classes, for which the only distinction is the color permutation of the unpaired steps. Therefore, we define the superclasses C_m, which contain the S^m equivalent classes c_m. The relationship between

the size of the superclass C_m, represented as N_m, and the size of the class c_m, represented as n_m, can be succinctly expressed by $N_m = S^m n_m$. With this understanding, we can simulate the distribution of C_m, and the expectation value $\langle \text{SWAP}_l \rangle$ can be estimated using the frequency Λ_m of each superclass C_m. Then the second-order Rényi EE is given by

$$s^{(2)} = -\ln \langle \text{SWAP}_A \rangle = -\ln \sum_m S^{-m} \Lambda_m^2. \tag{36}$$

For the colorless case, the Monte Carlo procedure directly samples the Motzkin configurations by repeatedly applying the Hamiltonian term Π^{exchange} to the Motzkin configurations. Specifically, at each step, a bond is randomly selected, and one of the operators $|D\rangle\langle D|$, $|U\rangle\langle U|$, or $|V\rangle\langle V|$ is applied to it. Once the initial state is a Motzkin state, the updated states generated by Π^{exchange} remain within the set of Motzkin states, and all Motzkin states are sampled with equal weight. As the projection operators Π^{boundary} and Π^{cross} are designed to project out non-Motzkin states, they are not required during the update process. The frequency Λ_m of configurations, with m being the midpoint height, is recorded as the measurement. For the colored case, sampling of spin-1 configurations can still be performed by identifying the different colors. However, the update rule for the exchange $\uparrow\downarrow \leftrightarrow 00$ must be modified using a Metropolis algorithm to ensure that the population ratio of $\uparrow\downarrow$ to 00 remains equal to S.

To calculate the Rényi EE of other Rényi indices, generally, we need to generalize the SWAP operator, and n replicas need to be sampled. However, our algorithm can be directly generalized to simulate the Rényi EE of any Rényi index n, where n could be any positive real number and is not constrained to be an integer, using the following formula:

$$s^{(n)} = \frac{1}{1-n} \ln \sum_{m=0}^{l} S^{-m(n-1)} \Lambda_m^n. \tag{37}$$

Additionally, this algorithm can be employed to determine the vN EE, which is given by

$$s^{\text{vN}} = -\sum_{m=0}^{l} \Lambda_m \ln (S^{-m} \Lambda_m). \tag{38}$$

B. Results of the EE from MC

The vN and Rényi EEs computed using the MC method are presented in this section. Figure 2 shows a comparison of our numerical results and the analytical results in Eqs. (6) and (8), demonstrating good agreement. The ratios converge to 1 as increasing $2l$, the system size.

The MC data of the Motzkin chain are analyzed using a fitting process. We fit the data using the form $a\sqrt{l} + b \ln l + \delta$, where a could be zero or not. Here, l represents the size of the subsystem, which is determined by making a cut at the midpoint of a chain with a size of $2l$. The results of coefficient a are presented in Fig. 3. For the vN EE, which is indicated by the point at $n = 1$, the numerical results closely align with the analytical predictions in Eq. (7). Furthermore, our findings indicate that the square-root term tends to diminish as n increases, consistent with the previous analysis in Eq. (29) that the Rényi EE does not include a $\sqrt{l}$ term. Figure 4 presents the results for coefficients b and δ, agreeing with analytical

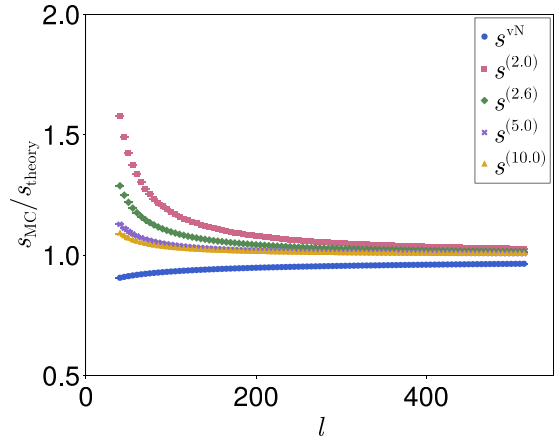

FIG. 2. The ratio of the EE results based on MC simulations and analytical calculations. The MC data are simulated on a two-color ($S = 2$) Motzkin chain of size $2l$, and the EEs are calculated on the subsystem by cutting at the midpoint. As the subsystem size l increases, the ratio tends to be 1, showing that the numerical and analytical results agree well for large system sizes.

calculations. Due to the finite-size effect, the fitted values of a, b, and δ deviate from theoretical predictions when $n > 1$. This effect arises from the competition between $(n-1)$ and $\sqrt{l}$. Consequently, the discrepancy between numerical and theoretical results becomes more pronounced for smaller n. The finite-size effect will be discussed in detail below.

We observe that there is an EE singularity of the Rényi index at $n = 1$, as indicated by both analytical and numerical results. The transition from a $\ln l$ scaling to a $\sqrt{l}$ scaling is

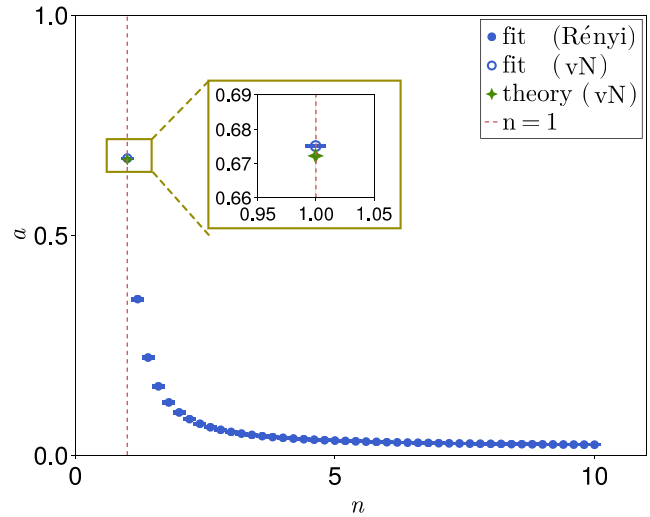

FIG. 3. The value of the coefficient of the $\sqrt{l}$ term a in EE for a two-color ($S = 2$) Motzkin chain. The MC data are sampled on system sizes from 80 to 1260 sites. The fitting results are illustrated as blue dots (for Rényi EE) and open circles (for vN EE) with error bars, which are fitted with the form $a\sqrt{l} + b \ln l + \delta$, where l is the subsystem size. The theoretical prediction for vN EE is shown as a green star. The vN EE has a finite value of a, which agrees with the theoretical prediction. The nonzero value of a for Rényi EE is caused by the finite-size effect.

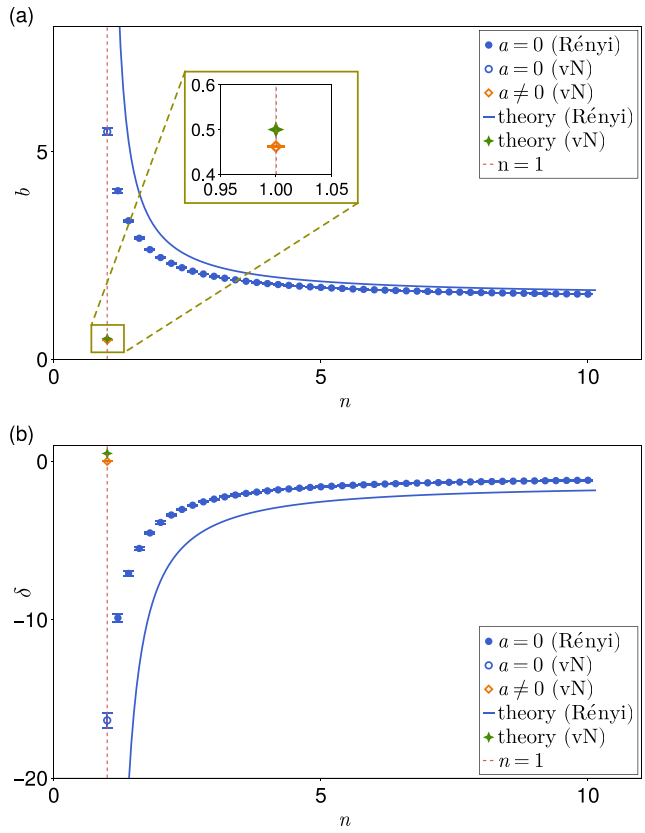

FIG. 4. The coefficient values in the scaling form of vN and Rényi EEs for the two-color Motzkin chain. The MC data are sampled on system sizes from 80 to 1260 sites for the both plots. The EE data are fitted by the form $b\ln l+\delta$, represented by the blue dots (for Rényi EE) and open circles (for vN EE) with error bars. vN EE data are also fitted by the form $a\sqrt{l}+b\ln l+\delta$, represented by the orange diamonds. The analytical results are also shown. (a) The value of b, the coefficient of the $\ln l$ term. (b) The value of the constant term δ.

governed by the second term in the expansion of the Rényi EE, as outlined in Eq. (12):

$$\frac{1}{1-n}\ln F_{2n}(p_1,p_2,l)\tilde{T}^{-n} = \frac{1}{1-n}\ln F_{2n}(p_1,p_2,l)F_2^{-n}(p_1,0,l). \tag{39}$$

The exact value of $F_{2n}(p_1,p_2,l)F_2^{-n}(p_1,0,l)$ can be determined in specific values of n and S. For the colorless ($S=1$) Motzkin chain, $p_2=0$. It can be proved that $F_{2n}(p_1,p_2,l)F_2^{-n}(p_1,0,l)>1$ and has an upper bound in the large-l limit; thus, Eq. (39) contributes a constant term to the scaling of EE. For the case with $S>1$, however, the value of $F_{2n}(p_1,p_2,l)F_2^{-n}(p_1,0,l)$ can be determined for specific values of $(n-1)\sqrt{l}$ in the large-l limit. It can be summarized as

$$F_{2n}(p_1,p_2,l)F_2^{-n}(p_1,0,l)=\begin{cases}0, & (n-1)\sqrt{l}\to+\infty,\\ 1, & (n-1)\sqrt{l}\to 0^+.\end{cases} \tag{40}$$

When analyzing the scaling of the Rényi entanglement entropy, we consider the limit $(n-1)\sqrt{l}\to\infty$. Following the discussion in the previous section, this leads to the first case in Eq. (40). For the vN EE, however, we must first take the limit $n\to 1$, in which case $(n-1)\sqrt{l}$ is always treated as zero. From the definition in Eq. (17), $\lim_{n\to1}F_{2n}(p_1,p_2,l)\to F_2(p_1,0,l)$, resulting in the second case in Eq. (40). These two distinct cases demonstrate that the limits $l\to\infty$ and $n\to1$ do not commute in the calculation of the EE. Furthermore, the condition in Eq. (40) determines whether the EE scales as $\sqrt{l}$ or $\ln l$. Equation (40) also accounts for the significant finite-size effects observed for small Rényi indices, as shown in Fig. 4. Since the theoretical result for the Rényi EE in Eq. (29) is valid only in the limit $(n-1)\sqrt{l}\to\infty$, numerical results for smaller Rényi indices exhibit larger deviations from Eq. (29).

As $n\to1$ (the vN EE) is the EE singularity of an infinite Motzkin spin chain, the finite-size modification becomes significantly large near $n=1$. This finite-size effect is dominated by the term $\frac{1}{(n-1)\sqrt{l}}$, which accounts for the considerable difference observed between the analytical results and the numerical results shown in Fig. 4 as n approaches 1.

From the perspective of the entanglement spectrum, the distinct scaling behavior of the vN EE compared to the Rényi EE originates from the abundance of highly excited levels. The EE can be interpreted as the thermal entropy of an entanglement Hamiltonian $H_E=-\ln\rho_A$, where ρ_A denotes the reduced density matrix. The entanglement spectrum ϵ_i corresponds to the eigenvalues of the entanglement Hamiltonian [25,77,78]. By definition, $\epsilon_i=-\ln\lambda_i$, where λ_i are the eigenvalues of ρ_A. For any Rényi index $n>1$, the Rényi EE exhibits identical scaling, including $s^{(\infty)}$, which is determined exclusively by the largest eigenvalues [79]. Since $s^{(n)}=\frac{1}{1-n}\ln\sum_i e^{-n\epsilon_i}$, smaller values of n lead to greater contributions from higher levels of the entanglement spectrum. The exponentially large population of these highly excited levels, illustrated in Fig. 5, ultimately results in the vN EE exhibiting a stronger scaling behavior than the Rényi EE.

V. DISORDER OPERATOR

The disorder operator [14,17,56,80–86] is a nonlocal operator capable of detecting higher-form symmetries, which are often challenging to measure using local operators. For a system with global symmetry, the DO is defined as the symmetry operator that acts on a specific subsystem. Recent research [18,19,22,58,60,87] has demonstrated that the DO exhibits universal scaling behavior in various quantum systems. Typically, the scaling behavior of the negative logarithm of the DO is similar to the scaling behavior of EE, which captures the essential information from CFT.

The Hamiltonian and the ground state of the colored Motzkin chain possess multiple symmetries [54]. First, the colored Motzkin chain has continuous $U(1)$ symmetry characterized by the charge $Q^z=\sum_j^{2l}S_j^z$, where $2l$ is the system size. Consequently, we define the DO as

$$X^z(\theta)=\prod_j^{l}e^{i\theta S_j^z}, \tag{41}$$

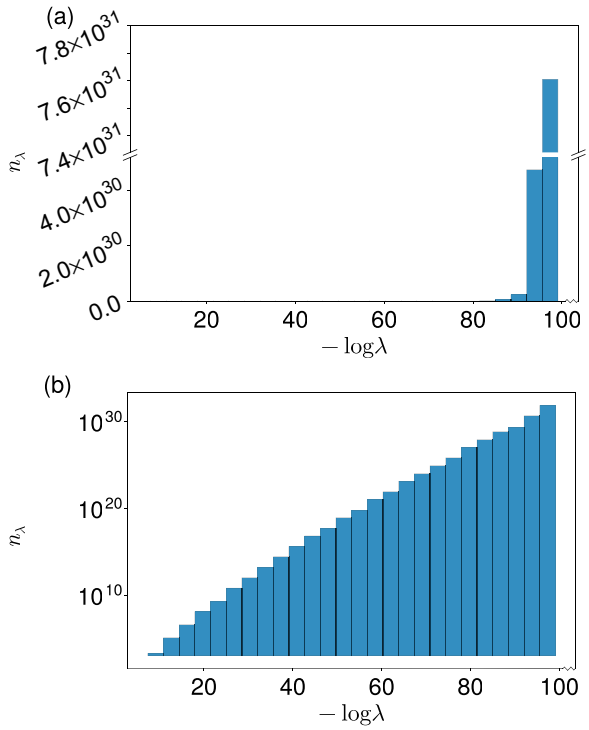

FIG. 5. The density of states in the entanglement spectrum, obtained with the reduced density matrix of a spin-2 Motzkin chain of size 1070. The horizontal axis $-\ln\lambda$ is the eigenvalue of the entanglement Hamiltonian (λ is the eigenvalue of the reduced density matrix ρ_A); the vertical axis is the density of states n_λ in a small window of $-\ln\lambda$, with natural and logarithmic scales used in (a) and (b), respectively.

which acts solely on half of the chain, which is obtained by cutting at the midpoint. λ_m in Eq. (10) is the possibility to get a height m at the midpoint when we identify different colors. Each of the m unpaired steps can be colored from 1 to S. Thus, the average of the DO is given by

$$\langle X^z(\theta)\rangle = \sum_{m=0}^{l} \lambda_m \left(\sum_{k=1}^{S} e^{ik\theta}\right)^m. \tag{42}$$

For large l, by substituting Eq. (10) into Eq. (42), setting $\xi = \frac{m}{\sqrt{l}}$, and utilizing the integral approximation, we arrive at the following expression for the DO:

$$\langle X^z(\theta)\rangle = \frac{1}{\tilde{T}} \int_0^\infty d\xi \xi^2 e^{-p_1(1,S)\xi^2} \left[\frac{\sin\left(\frac{S\theta}{2}\right)}{S\sin\frac{\theta}{2}}\right]^{\sqrt{l}\xi} e^{i\frac{S+1}{2}\theta\sqrt{l}\xi}, \tag{43}$$

where $\tilde{T}$ is defined in Eq. (23) and p_1 is defined in Eq. (16).

We define the following functions:

$$\chi_\alpha(\theta; S, l) = \int_0^\infty d\xi \xi^\alpha e^{-p_1(1,S)\xi^2} e^{y(\theta;S)\xi\sqrt{l}}, \tag{44}$$

$$y(\theta; S) = \ln\left[\frac{\sin\left(\frac{S\theta}{2}\right)}{S\sin\frac{\theta}{2}}\right] + i\frac{S+1}{2}\theta. \tag{45}$$

Then the DO can be expressed as $\langle X^z(\theta)\rangle = \chi_2/\tilde{T}$. It is easy to prove the following relations:

$$\frac{d}{dl}\chi_\alpha = \frac{y}{2\sqrt{l}}\chi_{\alpha+1}, \tag{46}$$

$$(\alpha+1)\chi_\alpha = -\sqrt{l}y\chi_{\alpha+1} + 2p_1\chi_{\alpha+2}. \tag{47}$$

Based on Eq. (46), we have

$$\chi_{\alpha+2} = \frac{2}{y^2}\frac{d}{dl}\chi_\alpha + \frac{4l}{y^2}\frac{d^2}{dl^2}\chi_\alpha. \tag{48}$$

Substituting Eqs. (46) and (48) into Eq. (47) yields

$$(\alpha+1)\chi_\alpha = \left(\frac{4p_1}{y^2} - 2l\right)\frac{d}{dl}\chi_\alpha + \frac{8p_1 l}{y^2}\frac{d^2}{dl^2}\chi_\alpha. \tag{49}$$

Now we look at Eq. (47). There are two possibilities for the large l scaling of χ_α: (1) χ_α and $\sqrt{l}\chi_{\alpha+1}$ have the same scaling order while $\chi_{\alpha+2}$ has a smaller order of l; (2) $\sqrt{l}\chi_{\alpha+1}$ and $\chi_{\alpha+2}$ have the same scaling order while χ_α has a smaller order of l. Other cases are impossible, which can be seen by writing down the recurrence relation of $\chi_{\alpha+1}$, $\chi_{\alpha+2}$, and $\chi_{\alpha+3}$. Then we have the following arguments for the two cases.

For the first case, $\chi_{\alpha+1} \sim \chi_\alpha/\sqrt{l}$. Substituting it into Eq. (46), we have

$$\frac{d}{dl}\chi_\alpha \sim \frac{y}{l}\chi_\alpha. \tag{50}$$

Thus, we can suppose that the scaling form of χ_α is

$$\chi_\alpha \sim l^\lambda, \tag{51}$$

and the value of λ can be determined by substituting Eq. (51) into Eq. (49):

$$(\alpha+1)l^\lambda = -2\lambda l^\lambda + \frac{8p_1}{y^2}\lambda(\lambda+1)l^{\lambda-1}, \tag{52}$$

which yields $\lambda = -(\alpha+1)/2$. Thus, the scaling form of χ_α is $\chi_\alpha \sim l^{-\frac{\alpha+1}{2}}$.

For the second case, $\chi_{\alpha+1} \sim \sqrt{l}\chi_\alpha$. Substituting it into Eq. (46), we have

$$\frac{d}{dl}\chi_\alpha \sim y\chi_\alpha. \tag{53}$$

So we can suppose that the leading term of the scaling form of χ_α is

$$\chi_\alpha \sim e^{\beta l} l^\lambda. \tag{54}$$

The values of β and λ can be determined by substituting Eq. (54) into Eq. (49):

$$(\alpha+1)l^\lambda = \left(-2\beta + \frac{8p_1}{y^2}\beta^2\right)l^{\lambda+1} + \left(\frac{4p_1}{y^2}\beta - 2\lambda + \frac{16p_1}{y^2}\beta\lambda\right)l^\lambda, \tag{55}$$

which yields

$$\beta = \frac{y^2}{4p_1}, \qquad \lambda = \frac{\alpha}{2}. \tag{56}$$

Thus, we have $\chi_\alpha \sim e^{\frac{y^2}{4p_1}l} l^{\frac{\alpha}{2}}$.

It is noteworthy that the DO is defined as an overlap of two states, which should have an upper bound. Thus, we can rule out the unphysical second case. Additionally, the numerical calculation of the integral in Eq. (44) and MC results in the following also support the first case. Under the conditions of the first case, we calculate the limit of the DO when $l \to \infty$ using Eqs. (46) and (47),

$$\lim_{l\to\infty} \frac{-\ln|\langle X^z(\theta)\rangle|}{\ln l} = -\lim_{l\to\infty} \frac{l\frac{d}{dl}\chi_2}{\chi_2} = \lim_{l\to\infty} \frac{-l\frac{1}{2\sqrt{l}}y\chi_3}{-\frac{\sqrt{l}}{3}y\chi_3 + 2p_1(1,S)\chi_4} = \frac{3}{2}. \tag{57}$$

Therefore, the scaling behavior of the negative logarithm of the DO is expressed as

$$-\ln|\langle X^z(\theta)\rangle| = \tfrac{3}{2}\ln l + \text{const.} \tag{58}$$

Note that the result holds for both the colorless and colored cases. The universal coefficient of the log term is $\frac{3}{2}$, the same as for the Rényi EE.

We calculate the DO numerically by using MC simulations, and the results for the cases with $S = 1, 2, 3$ are presented in Fig. 6. Figure 6 shows that the logarithmic scaling agrees well with the analytic result in Eq. (58).

The results presented in Eq. (58) hold true in the large-l limit. Since l is always paired with θ in Eq. (44), there is competition between small θ values and large l values. This competition leads to significant finite-size effects in the region of small θ. Our simulation also verifies this competition between θ and l. The DOs are fitted using the function $b\ln l + \text{const}$ based on the data for various segments of system sizes. The fitted results for b are shown in Fig. 7(a) for various θ values using different system size segments. Figure 7(a) reveals that for small θ, a significant deviation of b from $3/2$ occurs due to finite-size effects. However, this deviation decreases as the system size increases. This trend can be clearly observed by examining the fit results for a fixed θ_0 as the system size l increases, as presented in Fig. 7(b). Although the deviation initially grows with increasing l, the value of b ultimately converges to the analytical result of $3/2$.

In addition to the $U(1)$ symmetry above, the ground state of the Motzkin chain exhibits an additional $U(1)$ symmetry characterized by the charge $Q^c = \sum_j^{2l}\sum_k^S(|\uparrow^k\rangle_j\langle\uparrow^k| - |\downarrow^k\rangle_j\langle\downarrow^k|)$. Then the associated DO is

$$\langle X^c(\theta)\rangle = \left\langle \prod_j^l e^{\sum_k^S i\theta\left(|\uparrow^k\rangle_j\langle\uparrow^k| - |\downarrow^k\rangle_j\langle\downarrow^k|\right)} \right\rangle = \frac{1}{T}\sum_{m=0}^{l}\frac{m^2}{l}e^{-p_1(1,S)\frac{m^2}{l}}e^{ikm\theta}. \tag{59}$$

Based on a calculation similar to that for $\langle X^z\rangle$ above, in the limit of $l \to \infty$, the negative logarithm of $\langle X^c\rangle$ also has the $\ln l$ scaling behavior,

$$-\ln|\langle X^c(\theta)\rangle| = \tfrac{3}{2}\ln l + \text{const.} \tag{60}$$

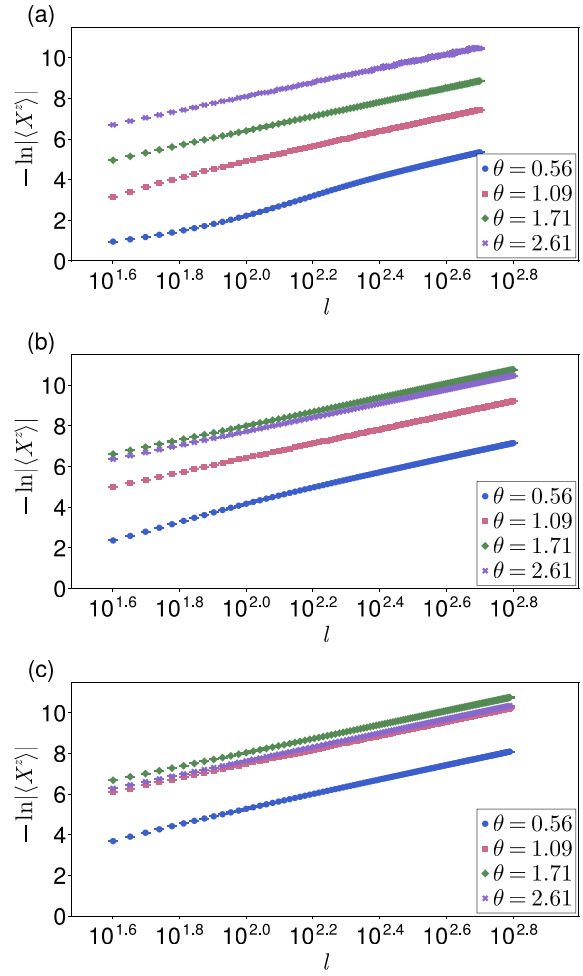

FIG. 6. The negative logarithmic DO under $U(1)$ symmetry with charge Q^z. The MC data are sampled on system sizes ranging from 80 to 1260 sites. The horizontal axis is the subsystem size l, determined by cutting at the midpoint of the chain. (a) Colorless Motzkin chain. (b) Two-color Motzkin chain. (c) Three-color Motzkin chain.

The numerical results are illustrated in Fig. 8.

The model also has a permutation symmetry with regard to different colors. For instance, as shown in Fig. 1, it remains a Motzkin walk even after the blue and pink steps are swapped. We introduce a DO of X^p that permutes colors within the subsystems. It can be proved that the expectation value of this DO equals λ_0 as outlined in Eq. (10), which can be estimated in the limit of large l as [52,54]

$$\begin{aligned}\langle X^p\rangle &= \lambda_0 \\ &= \frac{l^2}{(2\sqrt{S}+1)^{2l}T}\left(\sum_{i=0}^{l/2} S^i \frac{l!}{(i+1)!i!(l-2i)!}\right)^2 \\ &= \frac{l^2}{(2\sqrt{S}+1)^{2l}T}\left({}_2F_1\left(-\frac{l}{2},\frac{1}{2}-\frac{l}{2},2,4S\right)\right)^2 \\ &= l^{3/2}\left({}_2F_1\left(-l,\frac{3}{2},3,\frac{4\sqrt{S}}{2\sqrt{S}+1}\right)\right)^2,\end{aligned} \tag{61}$$

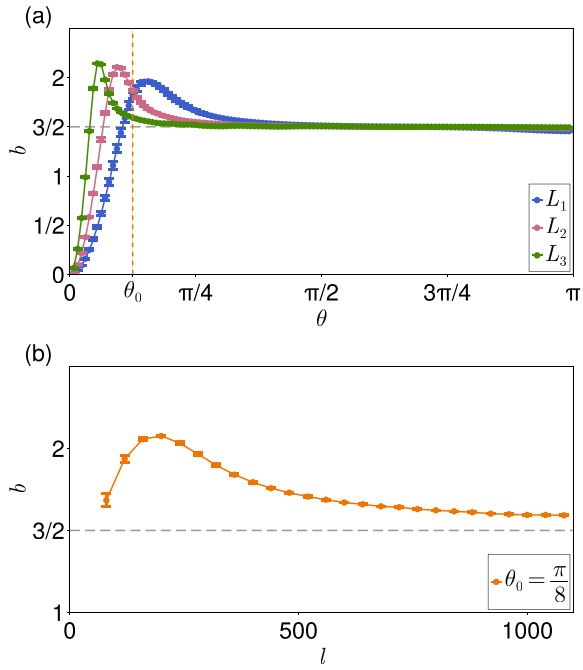

FIG. 7. The value of the coefficient b is obtained by fitting the data of $-\ln|\langle X^z(\theta)\rangle|$ to the form $b\ln l + \text{const}$, where the system under consideration is a two-color Motzkin chain. (a) The horizontal axis represents the phase θ associated with the $U(1)$ symmetry. The curves are obtained from fits over various system size ranges: L_1 spans from 80 to 310 sites, L_2 spans from 310 to 530 sites, and L_3 spans from 1030 to 1260 sites. The coefficient b approaches a value of $3/2$ as the system size increases. A notable finite-size effect arises due to the competition between θ and l, particularly in the small-θ region. This finite-size effect becomes less prominent as the system size l increases, as demonstrated in (b), which displays the fit results at $\theta_0 = \pi/8$. In (b), the horizontal axis l denotes the system size, where the value at each l is obtained by fitting data from system sizes ranging from l to $l + 160$ sites.

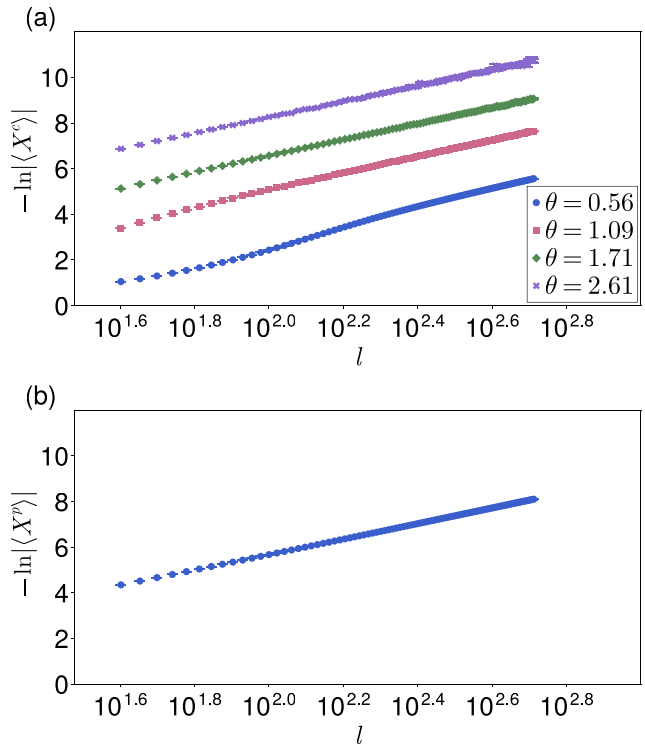

FIG. 8. The negative logarithms of DOs. The system is a two-color Motzkin chain, and the MC data are sampled on system sizes ranging from 80 to 1260 sites. The horizontal axis is the subsystem size l, obtained by cutting at the midpoint of the chain. (a) The DO of $U(1)$ symmetry with charge Q^c. (b) The DO of the permutation symmetry. The results in (a) and (b) support the universal coefficient of $\ln l$ term having a value of $3/2$.

where we used the relation $T = \sqrt{l}\tilde{T} \sim \sqrt{l}$ obtained from Eqs. (13) and (23). Here, ${}_2F_1$ represents the Gauss hypergeometric function, and the transformation relation between hypergeometric functions is utilized. In the large-l limit, the asymptotic form is [88]

$$\lim_{l\to\infty} {}_2F_1\left(-l, \frac{3}{2}, 3, \frac{4\sqrt{S}}{2\sqrt{S}+1}\right) = \frac{\Gamma(3)}{\Gamma(3/2)}\left((l+1)\frac{4\sqrt{S}}{2\sqrt{S}+1}\right)^{-3/2}. \tag{62}$$

Substituting it into Eq. (61), the negative logarithmic DO also exhibits logarithmic scaling:

$$-\ln|\langle X^p\rangle| = \tfrac{3}{2}\ln l + \text{const}. \tag{63}$$

We simulate this DO using the MC method. The results also support these findings and are presented in Fig. 8(b).

VI. SUMMARY AND DISCUSSION

It has generally been believed that the von Neumann entanglement entropy can be obtained through the analytic continuation of the Rényi index from Rényi entropy. However, the colored Motzkin chain serves as a counterexample, as the expression for the leading term of the Rényi entanglement entropy diverges at $n = 1$ and an extra leading term is needed for correction. We investigated the scaling behaviors of entanglement entropies theoretically and numerically to demonstrate the failure of analytic continuation. Mathematically, this singularity occurs because the limits $l \to \infty$ and $n \to 1$ cannot commute in the derivation procedures for the von Neumann and Rényi entanglement entropies, respectively. On the other hand, it can also be understood by the exponentially increasing density of states in its entanglement spectrum.

We also explored the scaling of the logarithms of disorder operators under different symmetries in colored Motzkin chains analytically and numerically. The analytic analysis predicts that all the logarithms of disorder operators exhibit the same scaling as Rényi entanglement entropy. Our numerical simulations also confirm these analytic calculations. The scaling of the Rényi entanglement entropy and the logarithms of the disorder operators point out that the coefficient of the $\ln l$ term is a universal fingerprint of the physics of Motzkin walks.

Although the entanglement entropy is difficult to measure in experiments, even in a small system [89,90], the disorder operator is an observable that can easily be extracted, particularly in cold atom platforms. We propose probing the constrained physics of Motzkin systems intrinsically via disorder operators in experiment.

ACKNOWLEDGMENTS

We thank M. Cheng for the great help with the analytical calculation. We also thank Z. H. Liu for the useful discussions. J.W. and C.W. are supported by the National Natural Science Foundation of China under Grants No. 12234016 and No. 12174317. Z.L. and Z.Y. acknowledge the start-up funding from Westlake University, the China Postdoctoral Science Foundation under Grant No. 2024M762935, and the NSFC Special Fund for Theoretical Physics under Grant No. 12447119. The authors thank the high-performance computing center of Westlake University and Beijing PARATERA Tech Co. for providing HPC resources. This work is supported by the New Cornerstone Science Foundation.

DATA AVAILABILITY

The data that support the findings of this article are openly available [63].

[1] L. Amico, R. Fazio, A. Osterloh, and V. Vedral, Entanglement in many-body systems, Rev. Mod. Phys. **80**, 517 (2008).
[2] N. Laflorencie, Quantum entanglement in condensed matter systems, Phys. Rep. **646**, 1 (2016).
[3] B. Zeng *et al.*, *Quantum Information Meets Quantum Matter* (Springer, New York, 2019).
[4] M. A. Nielsen and I. L. Chuang, *Quantum Computation and Quantum Information* (Cambridge University Press, Cambridge, 2010).
[5] M. M. Wilde, *Quantum Information Theory* (Cambridge University Press, Cambridge, 2013).
[6] A. Kitaev and J. Preskill, Topological entanglement entropy, Phys. Rev. Lett. **96**, 110404 (2006).
[7] M. Levin and X.-G. Wen, Detecting topological order in a ground state wave function, Phys. Rev. Lett. **96**, 110405 (2006).
[8] G. Vidal, J. I. Latorre, E. Rico, and A. Kitaev, Entanglement in quantum critical phenomena, Phys. Rev. Lett. **90**, 227902 (2003).
[9] V. E. Korepin, Universality of entropy scaling in one dimensional gapless models, Phys. Rev. Lett. **92**, 096402 (2004).
[10] Z. Wang, Z. Deng, Z. Wang, Y.-M. Ding, W. Guo, and Z. Yan, Probing phase transition and underlying symmetry breaking via entanglement entropy scanning, arXiv:2409.09942.
[11] P. Calabrese and A. Lefevre, Entanglement spectrum in one-dimensional systems, Phys. Rev. A **78**, 032329 (2008).
[12] E. Fradkin and J. E. Moore, Entanglement entropy of 2D conformal quantum critical points: Hearing the shape of a quantum drum, Phys. Rev. Lett. **97**, 050404 (2006).
[13] Z. Nussinov and G. Ortiz, Sufficient symmetry conditions for topological quantum order, Proc. Natl. Acad. Sci. USA **106**, 16944 (2009).
[14] Z. Nussinov and G. Ortiz, A symmetry principle for topological quantum order, Ann. Phys. (Amsterdam, Neth.) **324**, 977 (2009).
[15] H. Casini and M. Huerta, Universal terms for the entanglement entropy in 2+1 dimensions, Nucl. Phys. B **764**, 183 (2007).
[16] W. Ji and X.-G. Wen, Noninvertible anomalies and mapping-class-group transformation of anomalous partition functions, Phys. Rev. Res. **1**, 033054 (2019).
[17] W. Ji and X.-G. Wen, Categorical symmetry and noninvertible anomaly in symmetry-breaking and topological phase transitions, Phys. Rev. Res. **2**, 033417 (2020).
[18] L. Kong, T. Lan, X.-G. Wen, Z.-H. Zhang, and H. Zheng, Algebraic higher symmetry and categorical symmetry: A holographic and entanglement view of symmetry, Phys. Rev. Res. **2**, 043086 (2020).
[19] X.-C. Wu, W. Ji, and C. Xu, Categorical symmetries at criticality, J. Stat. Mech. (2021) 073101.
[20] W. Ding, N. E. Bonesteel, and K. Yang, Block entanglement entropy of ground states with long-range magnetic order, Phys. Rev. A **77**, 052109 (2008).
[21] Q.-C. Tang and W. Zhu, Critical scaling behaviors of entanglement spectra, Chin. Phys. Lett. **37**, 010301 (2020).
[22] J. Zhao, Z. Yan, M. Cheng, and Z. Y. Meng, Higher-form symmetry breaking at Ising transitions, Phys. Rev. Res. **3**, 033024 (2021).
[23] X.-C. Wu, C.-M. Jian, and C. Xu, Universal features of higher-form symmetries at phase transitions, SciPost Phys. **11**, 033 (2021).
[24] J. Zhao, B.-B. Chen, Y.-C. Wang, Z. Yan, M. Cheng, and Z. Y. Meng, Measuring Rényi entanglement entropy with high efficiency and precision in quantum Monte Carlo simulations, npj Quantum Mater. **7**, 69 (2022).
[25] Z. Yan and Z. Y. Meng, Unlocking the general relationship between energy and entanglement spectra via the wormhole effect, Nat. Commun. **14**, 2360 (2023).
[26] P. Calabrese and J. Cardy, Entanglement entropy and quantum field theory, J. Stat. Mech. (2004) P06002.
[27] Y.-M. Ding, Y. Tang, Z. Wang, Z. Wang, B.-B. Mao, and Z. Yan, Tracking the variation of entanglement Rényi negativity: A quantum Monte Carlo study, Phys. Rev. B **111**, L241108 (2025).
[28] Y.-M. Ding, J.-S. Sun, N. Ma, G. Pan, C. Cheng, and Z. Yan, Reweight-annealing method for evaluating the partition function via quantum Monte Carlo calculations, Phys. Rev. B **110**, 165152 (2024).
[29] M. A. Metlitski and T. Grover, Entanglement entropy of systems with spontaneously broken continuous symmetry, arXiv:1112.5166.
[30] Z. Deng, L. Liu, W. Guo, and H. Lin, Improved scaling of the entanglement entropy of quantum antiferromagnetic Heisenberg systems, Phys. Rev. B **108**, 125144 (2023).
[31] Z. Deng, L. Liu, W. Guo, and H.-Q. Lin, Diagnosing quantum phase transition order and deconfined criticality via entanglement entropy, Phys. Rev. Lett. **133**, 100402 (2024).

[32] Z. Wang, Z. Wang, Y.-M. Ding, B.-B. Mao, and Z. Yan, Bipartite reweight-annealing algorithm to extract large-scale data of entanglement entropy and its derivative in high precision, Nat. Commun. **16**, 5880 (2025).

[33] T. Grover, Y. Zhang, and A. Vishwanath, Entanglement entropy as a portal to the physics of quantum spin liquids, New J. Phys. **15**, 025002 (2013).

[34] J. Zhao, Y.-C. Wang, Z. Yan, M. Cheng, and Z. Y. Meng, Scaling of entanglement entropy at deconfined quantum criticality, Phys. Rev. Lett. **128**, 010601 (2022).

[35] M. Nozaki, T. Numasawa, and T. Takayanagi, Quantum entanglement of local operators in conformal field theories, Phys. Rev. Lett. **112**, 111602 (2014).

[36] J. Cardy and E. Tonni, Entanglement Hamiltonians in two-dimensional conformal field theory, J. Stat. Mech. (2016) 123103.

[37] P. Bueno, R. C. Myers, and W. Witczak-Krempa, Universality of corner entanglement in conformal field theories, Phys. Rev. Lett. **115**, 021602 (2015).

[38] H. Casini and M. Huerta, Positivity, entanglement entropy, and minimal surfaces, J. High Energy Phys. 11 (2012) 087.

[39] R. Longo and F. Xu, Von Neumann entropy in QFT, Commun. Math. Phys. **381**, 1031 (2021).

[40] P. Boes, J. Eisert, R. Gallego, M. P. Müller, and H. Wilming, Von Neumann entropy from unitarity, Phys. Rev. Lett. **122**, 210402 (2019).

[41] F. Giraldi and P. Grigolini, Quantum entanglement and entropy, Phys. Rev. A **64**, 032310 (2001).

[42] W. Donnelly, Decomposition of entanglement entropy in lattice gauge theory, Phys. Rev. D **85**, 085004 (2012).

[43] T. Cubitt, A. W. Harrow, D. Leung, A. Montanaro, and A. Winter, Counterexamples to additivity of minimum output p-Renyi entropy for p close to 0, Commun. Math. Phys. **284**, 281 (2008).

[44] G. Camilo, G. T. Landi, and S. Eliëns, Strong subadditivity of the Rényi entropies for bosonic and fermionic Gaussian states, Phys. Rev. B **99**, 045155 (2019).

[45] B. Collins and I. Nechita, Random quantum channels II: Entanglement of random subspaces, Rényi entropy estimates and additivity problems, Adv. Math. **226**, 1181 (2011).

[46] E. D'Hoker, X. Dong, and C.-H. Wu, An alternative method for extracting the von Neumann entropy from Rényi entropies, J. High Energy Phys. 01 (2021) 042.

[47] J. Fuentes and J. Gonçalves, Rényi entropy in statistical mechanics, Entropy **24**, 1080 (2022).

[48] M. Müller-Lennert, F. Dupuis, O. Szehr, S. Fehr, and M. Tomamichel, On quantum Rényi entropies: A new generalization and some properties, J. Math. Phys. **54**, 122203 (2013).

[49] A. Dutta, G. Aeppli, B. K. Chakrabarti, U. Divakaran, T. F. Rosenbaum, and D. Sen, *Quantum Phase Transitions in Transverse Field Spin Models: From Statistical Physics to Quantum Information* (Cambridge University Press, Cambridge, 2015).

[50] J. Eisert, M. Cramer, and M. B. Plenio, *Colloquium*: Area laws for the entanglement entropy, Rev. Mod. Phys. **82**, 277 (2010).

[51] S. T. Flammia, A. Hamma, T. L. Hughes, and X.-G. Wen, Topological entanglement Rényi entropy and reduced density matrix structure, Phys. Rev. Lett. **103**, 261601 (2009).

[52] R. Movassagh and P. W. Shor, Supercritical entanglement in local systems: Counterexample to the area law for quantum matter, Proc. Natl. Acad. Sci. USA **113**, 13278 (2016).

[53] F. Sugino and V. Korepin, Rényi entropy of highly entangled spin chains, Int. J. Mod. Phys. B **32**, 1850306 (2018).

[54] V. Menon, A. Gu, and R. Movassagh, Symmetries, correlation functions, and entanglement of general quantum Motzkin spin-chains, arXiv:2408.16070.

[55] E. Lake, Higher-form symmetries and spontaneous symmetry breaking, arXiv:1802.07747.

[56] E. Fradkin, Disorder operators and their descendants, J. Stat. Phys. **167**, 427 (2017).

[57] Z. Liu, R.-Z. Huang, Y.-C. Wang, Z. Yan, and D.-X. Yao, Measuring the boundary gapless state and criticality via disorder operator, Phys. Rev. Lett. **132**, 206502 (2024).

[58] Y.-C. Wang, M. Cheng, and Z. Y. Meng, Scaling of the disorder operator at $(2+1)d$ U(1) quantum criticality, Phys. Rev. B **104**, L081109 (2021).

[59] Y.-C. Wang, N. Ma, M. Cheng, and Z. Y. Meng, Scaling of the disorder operator at deconfined quantum criticality, SciPost Phys. **13**, 123 (2022).

[60] W. Jiang, B.-B. Chen, Z. H. Liu, J. Rong, F. F. Assaad, M. Cheng, K. Sun, and Z. Y. Meng, Many versus one: The disorder operator and entanglement entropy in fermionic quantum matter, SciPost Phys. **15**, 082 (2023).

[61] Z. H. Liu, W. Jiang, B.-B. Chen, J. Rong, M. Cheng, K. Sun, Z. Y. Meng, and F. F. Assaad, Fermion disorder operator at Gross-Neveu and deconfined quantum criticalities, Phys. Rev. Lett. **130**, 266501 (2023).

[62] Z. H. Liu, Y. Da Liao, G. Pan, M. Song, J. Zhao, W. Jiang, C.-M. Jian, Y.-Z. You, F. F. Assaad, Z. Y. Meng, and C. Xu, Disorder operator and Rényi entanglement entropy of symmetric mass generation, Phys. Rev. Lett. **132**, 156503 (2024).

[63] Jerryemc, Jerryemc/Motzkin_data: MotzkinWalkData, Zenodo (2025), https://doi.org/10.5281/zenodo.16454506.

[64] T. Motzkin, Relations between hypersurface cross ratios, and a combinatorial formula for partitions of a polygon, for permanent preponderance, and for non-associative products, Bull. Am. Math. Soc. **54**, 352 (1948).

[65] R. Donaghey and L. W. Shapiro, Motzkin numbers, J. Comb. Theory, Ser. A **23**, 291 (1977).

[66] S. Bravyi, L. Caha, R. Movassagh, D. Nagaj, and P. W. Shor, Criticality without frustration for quantum spin-1 chains, Phys. Rev. Lett. **109**, 207202 (2012).

[67] M. B. Hastings, I. González, A. B. Kallin, and R. G. Melko, Measuring Renyi entanglement entropy in quantum Monte Carlo simulations, Phys. Rev. Lett. **104**, 157201 (2010).

[68] S. Humeniuk and T. Roscilde, Quantum Monte Carlo calculation of entanglement Rényi entropies for generic quantum systems, Phys. Rev. B **86**, 235116 (2012).

[69] S. Inglis and R. G. Melko, Wang-Landau method for calculating Rényi entropies in finite-temperature quantum Monte Carlo simulations, Phys. Rev. E **87**, 013306 (2013).

[70] P. Broecker and S. Trebst, Rényi entropies of interacting fermions from determinantal quantum Monte Carlo simulations, J. Stat. Mech. (2014) P08015.

[71] D. J. Luitz, X. Plat, N. Laflorencie, and F. Alet, Improving entanglement and thermodynamic Rényi entropy measurements in quantum Monte Carlo, Phys. Rev. B **90**, 125105 (2014).

[72] J. Pei, S. Han, H. Liao, and T. Li, The Rényi entanglement entropy of a general quantum dimer model at the RK point: A highly efficient algorithm, J. Phys.: Condens. Matter **26**, 035601 (2014).

[73] L. Wang and M. Troyer, Renyi entanglement entropy of interacting fermions calculated using the continuous-time quantum Monte Carlo method, Phys. Rev. Lett. **113**, 110401 (2014).
[74] F. F. Assaad, Stable quantum Monte Carlo simulations for entanglement spectra of interacting fermions, Phys. Rev. B **91**, 125146 (2015).
[75] J. D'Emidio, Entanglement entropy from nonequilibrium work, Phys. Rev. Lett. **124**, 110602 (2020).
[76] X. Zhou, Z. Y. Meng, Y. Qi, and Y. Da Liao, Incremental SWAP operator for entanglement entropy: Application for exponential observables in quantum Monte Carlo simulation, Phys. Rev. B **109**, 165106 (2024).
[77] Z. Liu, R.-Z. Huang, Z. Yan, and D.-X. Yao, Demonstrating the wormhole mechanism of the entanglement spectrum via a perturbed boundary, Phys. Rev. B **109**, 094416 (2024).
[78] C. Li, R.-Z. Huang, Y.-M. Ding, Z. Y. Meng, Y.-C. Wang, and Z. Yan, Relevant long-range interaction of the entanglement hamiltonian emerges from a short-range gapped system, Phys. Rev. B **109**, 195169 (2024).
[79] H. Wilming, M. Goihl, I. Roth, and J. Eisert, Entanglement-ergodic quantum systems equilibrate exponentially well, Phys. Rev. Lett. **123**, 200604 (2019).
[80] L. P. Kadanoff and H. Ceva, Determination of an operator algebra for the two-dimensional Ising model, Phys. Rev. B **3**, 3918 (1971).
[81] F. J. Wegner, Duality in generalized Ising models and phase transitions without local order parameters, J. Math. Phys. **12**, 2259 (1971).
[82] E. Fradkin and L. Susskind, Order and disorder in gauge systems and magnets, Phys. Rev. D **17**, 2637 (1978).
[83] A. Kapustin and N. Seiberg, Coupling a QFT to a TQFT and duality, J. High Energy Phys. 04 (2014) 001.
[84] D. Gaiotto, A. Kapustin, N. Seiberg, and B. Willett, Generalized global symmetries, J. High Energy Phys. 02 (2015) 172.
[85] X.-G. Wen, *Colloquium*: Zoo of quantum-topological phases of matter, Rev. Mod. Phys. **89**, 041004 (2017).
[86] X.-G. Wen, Choreographed entanglement dances: Topological states of quantum matter, Science **363**, eaal3099 (2019).
[87] W. Witczak-Krempa, Entanglement susceptibilities and universal geometric entanglement entropy, Phys. Rev. B **99**, 075138 (2019).
[88] N. M. Temme, Uniform asymptotic expansion for a class of polynomials biorthogonal on the unit circle, Constr. Approx. **2**, 369 (1986).
[89] R. Islam, R. Ma, P. M. Preiss, M. Eric Tai, A. Lukin, M. Rispoli, and M. Greiner, Measuring entanglement entropy in a quantum many-body system, Nature (London) **528**, 77 (2015).
[90] D. A. Abanin and E. Demler, Measuring entanglement entropy of a generic many-body system with a quantum switch, Phys. Rev. Lett. **109**, 020504 (2012).